Nanotechnology

PAPER

On the real-time atomistic deformation of nano twinned CrCoFeNi high entropy alloy

To cite this article: Shaohua Yan *et al* 2020 *Nanotechnology* **31** 385705

IOP Publishing Nanotechnology
Nanotechnology **31** (2020) 385705 (10pp) https://doi.org/10.1088/1361-6528/ab99ef

On the real-time atomistic deformation of nano twinned CrCoFeNi high entropy alloy

Shaohua Yan[1], **Qing H Qin**[2] **and Zheng Zhong**[1]

[1] School of Science, Harbin Institute of Technology, Shenzhen 518055, People's Republic of China
[1] Research School of Electrical, Energy and Materials Engineering, College of Engineering and Computer Science, The Australian National University ACT 2601, Australia

E-mail: qinghua.qin@anu.edu.au and zhongzheng@hit.edu.cn

Received 24 February 2020, revised 12 April 2020
Accepted for publication 5 June 2020
Published 3 July 2020

Abstract

High entropy alloys (HEAs) holding several principal elements in high concentration have unprecedented combination properties. The design of strong and highly ductile HEAs has attracted extensive attention from researchers in the last decade, such as in mechanisms for inducing different types of phase and nano-sized precipitates. Since some HEAs have low stacking fault energy, nanotwins can form during the plastic deformation process or magnetron sputtering, resulting in enhanced mechanical properties due to the existence of twin boundaries. The addition of twin boundaries is implied to be a promising method in engineering HEAs. Understanding how these twin boundaries affect the mechanical properties of nanotwinned HEAs is the key to designing strong and ductile examples. In this study, we performed a large-scale molecular dynamic simulation to investigate the mechanical properties of HEAs with different twin boundary spacings at various temperatures. The results show that the strength of HEAs at all tested temperatures increases with decreasing twin boundary spacing until a lower critical value of 1.83 nm is reached, which is close to the experimental value (2 nm). The strength of the HEAs at all tested temperatures decreases as the twin boundary spacing is decreased further. The dislocation motion transitions at the critical twin boundary spacing. In the sample with a twin boundary spacing bigger than 1.83 nm, Shockley dislocations tend to intersect the twin boundaries and glide in the hardening modes; on the other hand, Shockley dislocations travel along the direction parallel to the twin boundaries in samples with a twin boundary spacing smaller than 1.83 nm, leading to detwinning and softening in the HEAs. The dislocation motion and entanglement at 1 K are respectively slower and stronger than those at 300 K; the grain boundary activity is more obvious at a higher temperature. A mechanistic theoretical model together with a Hall–Petch relationship is then proposed to consider the coupled twin boundary and temperature effect on the deformation of nanotwinned HEAs.

Supplementary material for this article is available online

Keywords: high entropy alloys, molecular dynamics, nanotwin

(Some figures may appear in colour only in the online journal)

1. Introduction

Unlike traditional alloys, which contain one or two principle elements(e.g. Al is the main element in Al alloys [1, 2]), a new alloy consisting of at least five primary elements, named a high entropy alloy (HEA), has been attracting extensive attention from the academic community in the last decade [3, 4]. HEAs are known to be able to negate the existing trade-off

between strength and ductility; specifically, they can possess high strength without sacrificing too much ductility, and vice versa. Also, the performance of HEAs at low temperature is astounding due to their enhanced strength and ductility. Basically, the thermal activation in a traditional alloy is reduced at lower temperatures, which directly causes difficulties due to the activity of defects (e.g. stacking faults, dislocations and twinning). Consequently, the performance of traditional alloys at lower temperatures is not as good as that at room temperature, and is sometimes even worse [5]. However, CrCoFeMnNi HEAs consisting of single face centered cubic (FCC) phases are found to have better properties at 77 K with 1.2 GPa tensile strength and 70% ductility [6], compared to those at room temperature. The improved performance of CrCoFeMnNi HEAs is attributed to mechanical nanotwinning at cryogenic temperatures [6].

At room temperature, the ultimate tensile stress (UTS) of FCC single-phase HEAs is about 700 MPa. To increase its UTS, one strategy is to include body-centered cubic- (BCC) or HCP-structured phases or nanoscale precipitates in the HEA [7]. The hardness of the FCC phase in the HEA generally ranges from 1–2 GPa. Including certain percentages of BCC phases in the HEA can increase its hardness up to 6.55 GPa. For instance, the addition of Al to a CoCrFeNi system can lead to two-phase (FCC and BCC) HEAs, and the resultant UTS can reach up to 1.3 GPa with the ductility reduced below 10% [8]. The second method is to add HEAs with interstitial elements like carbon [9], hydrogen [10] and oxygen [11]. It is reported that the UTS and ductility of TiZrHfNb HEA was enhanced respectively by 48.5% and 95.2% via doping of about 2 at.% oxygen [11]. A small amount of carbon and hydrogen can also increase the yield stress and UTS in some HEAs [9, 10, 12]. Another way to improve the mechanical performance of HEAs is grain boundary (GB) engineering, by which the grain size is reduced or a heterogenous microstructure can be achieved. A smaller grain size is beneficial in improving the yield and UTS of HEAs [7, 12–16], and is consistent with the Hall–Petch relationship.

For HEAs with a relatively low stacking fault energy, their mechanical twins can be produced via an extensive plastic deformation process [17], and nanosized grains can be achieved at the same time; therefore the mechanical properties can be well improved while maintaining good ductility [18]. Apart from the plastic deformation process, extensive twins can be formed during magnetron sputtering [19, 20]. The introduction of twins in HEAs has also been found to increase the mechanical properties in HEA [12]. The coherent interface, twin boundary, can enhance the UTS of alloys without sacrificing ductility [21], and enhances material fatigue resistance [22]. However, softening is also reported in nanotwinned HEAs when the twin boundary spacing (λ) is 2 nm [19]. For nanotwinned copper, the strength increases with decreasing λ when $\lambda \leqslant 15$ nm, and then decreases while further decreasing λ. Yet there are no reports regarding the amount of λ at which this softening–strengthening transition will happen in nanotwinned HEAs.

To date, the effect of a twin boundary (TB) on the mechanical behavior of HEAs is yet to have been investigated systematically, hampering the use of this powerful engineering mechanism for strengthening the HEA. In this study, we systematically investigate the effect of λ on the deformation of nanotwinned HEAs via a molecular dynamic (MD) simulation. Since temperature can also influence the mechanical performance of nanotwinned materials [23], the temperature factor is also included in this study. The real-time atomistic deformation has been deeply explored to reveal the strengthening and softening mechanisms in nanotwinned HEAs. Moreover, a mechanistic theoretical model is proposed to explain the coupled TB and temperature effect on the mechanical behavior of nanotwinned HEAs. This research aims to provide insights into the design of strong and ductile HEAs with nanoscale twins.

2. Simulation methods

Each equiatomic CoCrFeNi type HEA sample for MD simulation contained 10 grains built via the Voronoi method [24]. As illustrated in figure 1, in step 1, a single crystal (SC) with different nanotwin spacings was first constructed; then, in step 2, combining the Voronoi method with the nanotwinned SC obtained in step 1, nanotwinned polycrystals were constructed. These samples were assumed to have dimensions of $20 \times 20 \times 20$ nm^3 and contain about 730 000 atoms. To study the effect of λ on the mechanical properties, the crystal orientation in each grain remained unchanged, only λ was altered, as demonstrated in figure s1 (available online at stacks.iop.org/NANO/31/385705/mmedia) in the supplementary materials. Five types of sample with different λ (i.e. 0.61 nm, 1.22 nm, 1.83 nm, 2.44 nm, and 3.05 nm) were constructed for simulation via LAMMPS [25–27]. The embedded atom method potential was adopted for the Co-Cr-Fe-Ni type HEA in this study [28]. The potential was chosen for the following two reasons: (1) the availability of the potentials, (2) the efficiency and computational time for MD simulation. Each sample was equilibrated for 300 ps under an NPT ensemble at a temperature of 300 K, 800 K, and 1200 K. In 1 K conditions, the sample was first equilibrated at 300 K for 300 ps, then quenched to 1 K for 200 ps, and finally relaxed at 1 K for another 100 ps. After the equilibration process, tensile loading was applied along the y axis with a strain rate of 1×10^9 s^{-1} to a final strain of 12%.

Periodic boundary conditions were applied in all three directions (x, y, and z axis) through the simulation. The timestep was kept as 1 fs in the simulation. The yield stress was calculated from the average stress at strains ranging from 2%–6%. To explore the deformation mechanisms and defect evolutions during plastic deformation, two different methods were used. Common neighbor analysis was used to assign different colors and identify different types of atom [29, 30]: green for FCC atoms, red for HCP atoms, and white for atoms in GBs or dislocation cores. The other one was a spatial-position-based method which assigns the color to the atoms according to their spatial position.

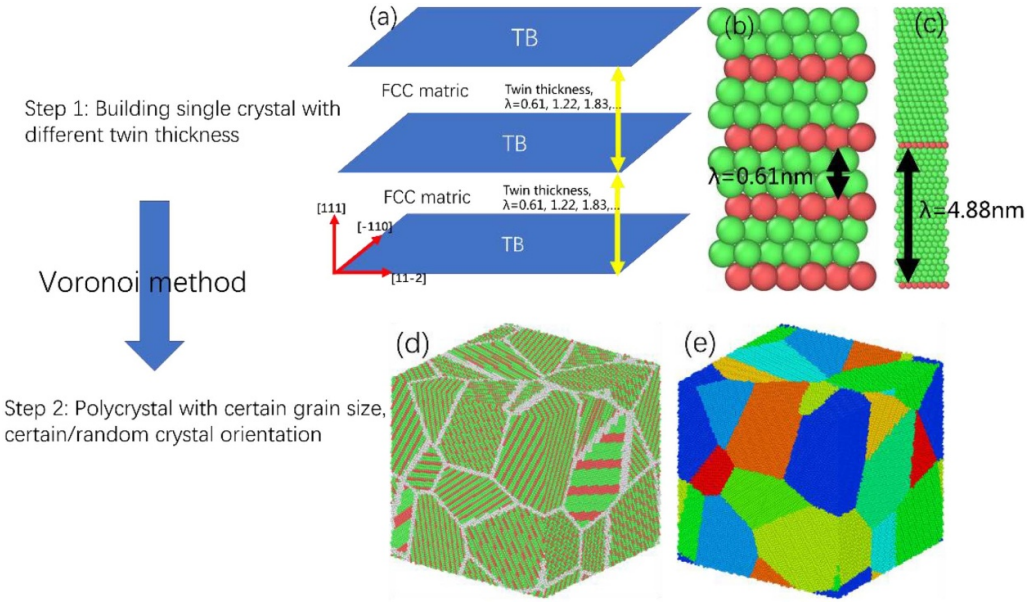

Figure 1. Diagram of the building of the MD model, (a)–(c) the construction of the nanotwinned single crystal with different λ, (d)–(e) a typical built MD polycrystal model with $\lambda = 0.61$ nm.

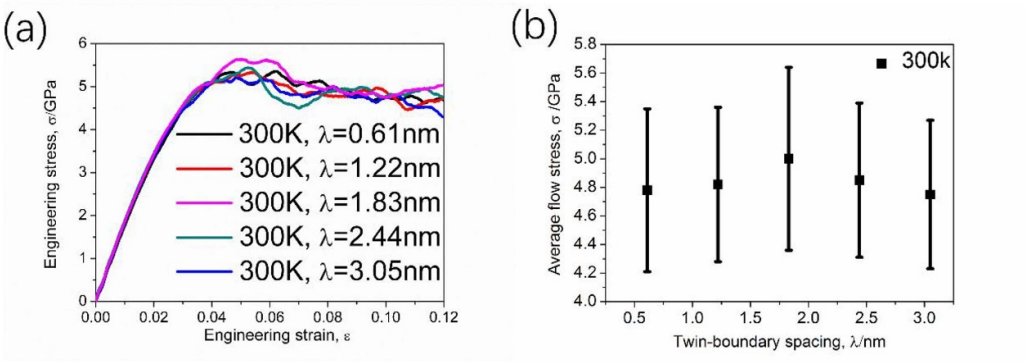

Figure 2. (a) Engineering stress–strain curves of nanotwinned HEA with different twin spacing (from 0.61 nm to 3.05 nm), (b) the average flow stress for samples with different twin boundary spacing.

3. Results

3.1. Effect of nanotwin boundary spacing

Figure 2(a) shows the engineering stress–strain curves of the samples varies with λ at a temperature of 300 K. All the stress–strain curves exhibit a drop in stress after reaching maximum stress, a phenomenon which is commonly found in MD simulations and attributed to the nucleation of dislocations [1, 30]. Figure 2(b) shows that the stress increases with decreasing λ, reaching a maximum stress at a critical λ ($\lambda = 1.83$ nm), and the stress decreases slightly with further decreasing λ. The critical λ is very close to the experimental one which is 2 nm [19].

The deformation mechanisms involved are revealed in figure 3, in which the state of the samples at 0% strain is also shown for better illustration of the deformation process. When $\lambda = 0.61$ nm, the dominant mechanism is detwinning, a change of λ in some grains, as indicated in areas in dark-dashed circles in figure 3(b) (more details can be seen in the movie s1 in the supplementary materials). With increasing λ, partial dislocations (Shockley dislocations) interacting with the twin boundary planes become dominant, as demonstrated in areas in figure 3(d) (blue-dashed square) and figure 3(f) (dark-dashed square). To further explore the dislocation behavior in different twin spacing samples, the detailed structure of dislocations in the grain is illustrated in figure 4. For the sample with $\lambda = 0.61$ nm (figures 4(a)–(c)) the Shockley dislocations are born in the junction between the GB and TB, and then travel parallel to the TB (more details in movie s2 in the supplementary materials). Such a moment of dislocation leads to detwinning and no interaction between dislocations since most dislocations are parallel to each other (see figure 4(c)). Such types of dislocation movement are also found in other grains, as seen in figure s2 in the supplementary materials.

However, dislocations in samples with larger λ (e.g. $\lambda = 1.83$ nm) behave in a different manner. As illustrated in figure 4(e), the dislocations interact with the TB after nucleating from the junctions between the GB and TB. Furthermore, these dislocations are not parallel to each other,

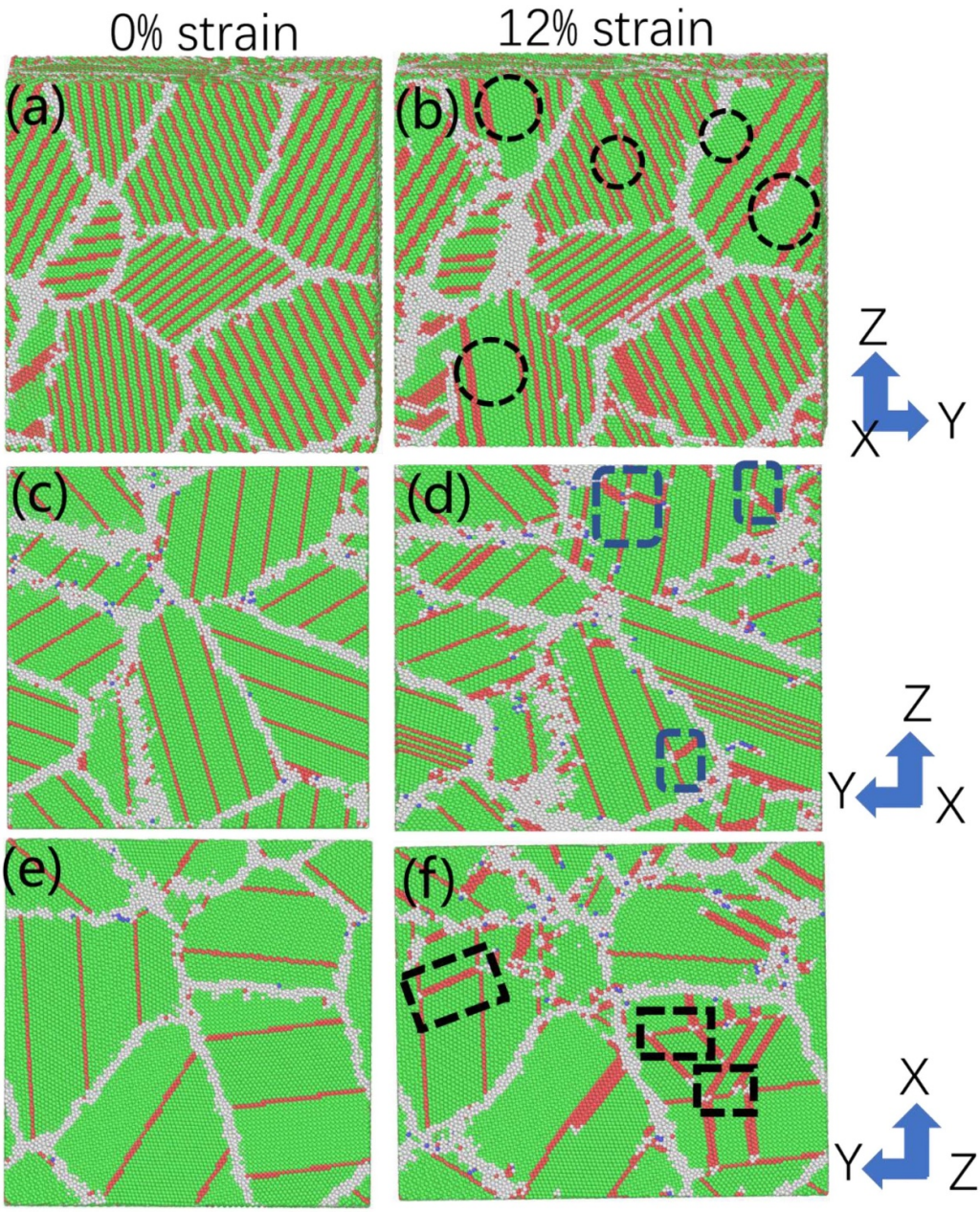

Figure 3. The deformation mechanisms of samples with different twin boundary spacings at 300 K, (a) and (b) for the sample with $\lambda = 0.62$ nm, (c) and (d) for the sample with $\lambda = 1.83$ nm, (e) and (f) for the sample with $\lambda = 3.05$ nm. The color of the atoms is assigned by common neighbor analysis: green for fcc atoms, red for atoms on the TB or stacking fault, white for atoms on the GBs or dislocation cores.

resulting in their entanglement (see figure 4(f)). More details of the dislocation structure in samples with a different λ can be found in figure s3 and movie 3 in the supplementary materials.

3.2. Effect of temperature

The engineering stress–strain curves of nanotwinned HEAs at different temperatures are shown in figures 5(a)–(d). For samples with a given λ (see figure 5(e)), the stress decreases with increasing temperature. The coupled effect of temperatures and λ on the yield stress is shown in figure 5(f). Similar to the trend found at 300 K, the stresses of all the simulated samples increase with decreasing λ before reaching a critical λ (i.e. 1.83 nm for all cases), then decrease slightly when further reducing λ.

Further effort has been made to reveal the deformation mechanisms at different temperatures. In the sample with $\lambda = 0.61$ nm at higher temperatures (i.e. 800 K), the migration of the GB plays a critical role in accommodating the plastic deformation apart from detwinning, as demonstrated in figure 6. Moreover, detwinning seems to happen quickly with an increasing temperature (see the white circled area in figures 6(b)–(d)). The distribution of shear strain near the GBs is displayed in figure 7, which clearly shows that higher strains are located near the GBs, and such strains are greater at higher temperatures, as indicated by dark arrows in figures 7(b)–(d).

The dislocation behavior in the same grain at different temperatures is shown in figure 8. At 1 K (figures 8(a)–(c)), the dislocation takes 10 ps from emission to absorption by the GB,

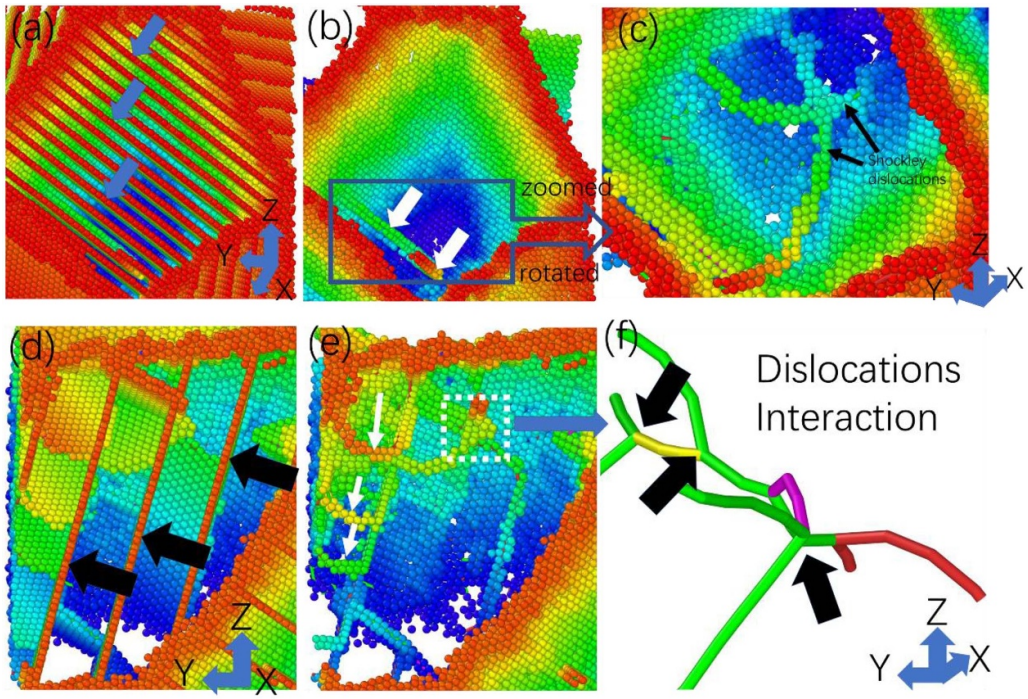

Figure 4. An atomistic view of the dislocation evolution of samples with different twin boundary spacings; (a)–(c) for the sample with $\lambda = 0.62$ nm, (d)–(f) for the sample with $\lambda = 1.83$ nm. The twin boundaries are shown in (a) and (d), as indicated by arrows. For clarity, the twin boundaries are invisible in the other images. Only non-FCC atoms are shown. The color of the atoms is given according to their spatial coordinate position.

while this process occurs much quickly (~5 ps) at 300 K. This finding suggests that the motion of dislocations is slower at low temperatures. Such slow motion may lead to dislocation entanglement (see movie s4 in the supplementary material), leading to higher dislocation density as a result, as evidenced by figures 8(g) and (h).

4. Discussions

The present research investigates the effect of nanotwins on the strength of HEAs, and it has been found that the strength of nanotwinned HEA is λ-dependent. To further reveal the deformation mechanism in this study, a schematic of the dislocation behaviors in samples with different λ is illustrated in figure 9. When λ is small (e.g. 0.61 nm shown in figures 9(a) and (b)), the Shockley dislocations glide in the direction parallel to the TB (white arrow in figure 9(b)). This type of dislocation motion is called 'soft mode' (figure 9(c)). As shown in the double Thompson tetrahedra (figure 9(d)), this mode may happen in the ABC plane in directions of AB, AC, and BC. The corresponding crystal slip systems include (111) $[\bar{1}10]$, (111) $[01\bar{1}]$, (111) $[10\bar{1}]$. With a bigger λ (e.g. 1.83 nm shown in figures 9(e) and (f)), the dislocations glide in several different directions and planes, as indicated by the white arrows in figures 9(e) and (f). These slip modes are called the hardening mode, as illustrated in figure 9(g). The slip systems in the hardening modes are shown in the double Thompson tetrahedra (figure 9(d)), indicating {111}<110> slip systems in these hardening modes. Under such hardening modes, dislocations can accumulate around the TBs, and interact with each other and the TBs, resulting in a high dislocation density (ρ) in the samples. The yield/flow stress can be calculated by $\sigma = Mab\sqrt{\rho}$; thus, the sample with dislocations gliding in the hardening modes presents greater yield/flow stress. Clearly, there is a deformation mechanism transition at a critical λ, which is determined by the mode of dislocation interaction with the TBs.

In accordance with the revealed deformation mechanisms in samples with different λ, a theoretical model is proposed considering λ and the temperature effect. Following the original work of Gao [23, 31], Zhu [32], and others [33], the macroscopic shear strain rate ($\dot{\varepsilon}$) under the plastic strain of b/λ can be expressed as:

$$\dot{\varepsilon} = \beta n \frac{b}{\lambda} \bar{\vartheta} \tag{1}$$

where β accounts for the contribution from Taylor factors and all possible slip systems, n is the active dislocation source, b is the magnitude of the Burger vector, ϑ is the dislocation nucleation rate, and λ is the TB spacing, which ranges from 0.61–3.05 nm in this study.

Since the dislocation is emitted from the junction between the GB and TB, as demonstrated in figures 4 and 9, the active dislocation source can be estimated by:

$$n = f_{(1)} \frac{d}{b} \tag{2}$$

where $f_{(1)}$ is the percentage of atoms that can act as effective dislocation nucleation sites, the value of $f_{(1)}$ ranges from 0–1; d is the grain size, which is 10 nm in this study.

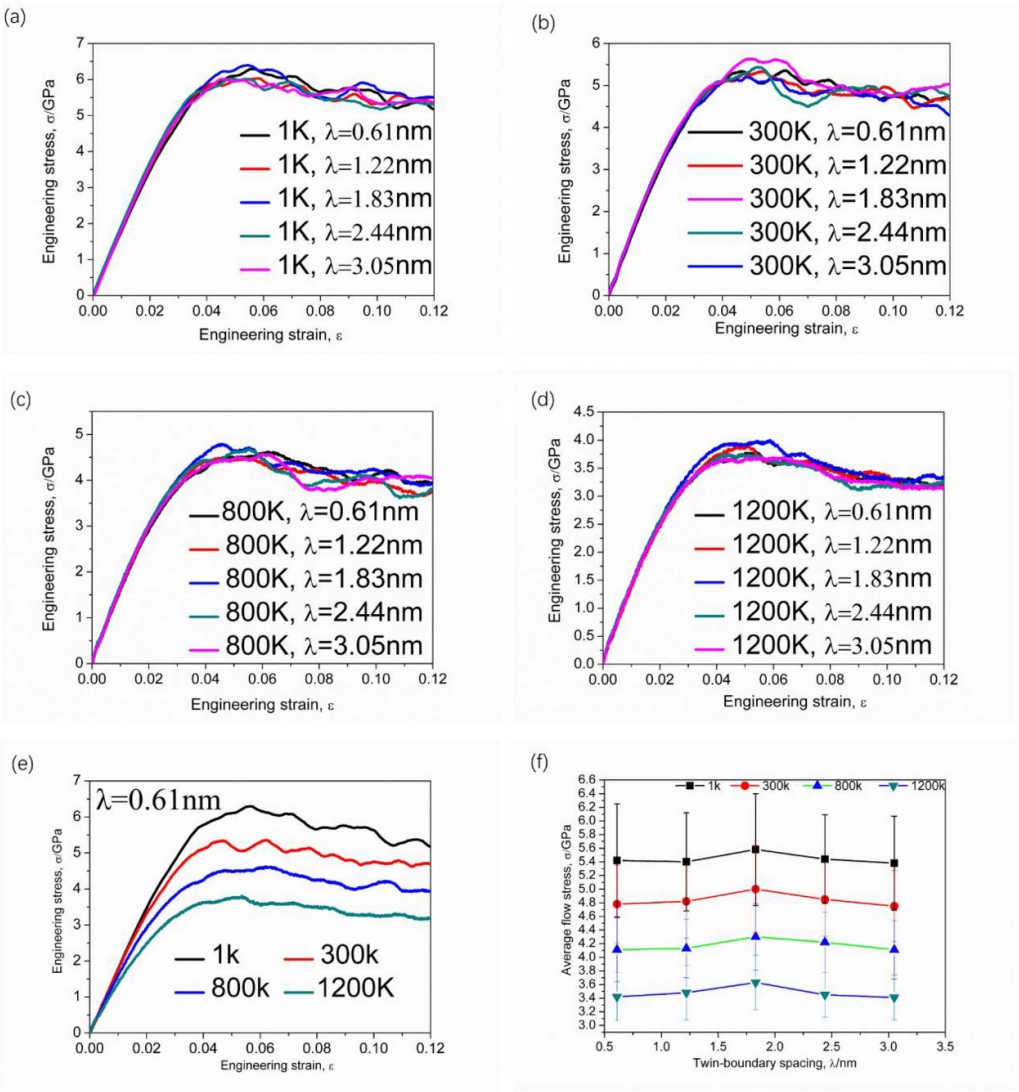

Figure 5. Engineering stress–strain curves of samples with different twin spacings at temperatures of 1 K (a), 300 K (b), 800 K (c), and 1200 K (d); (e) shows the stress–strain curves of the sample with $\lambda = 0.61$ nm at different temperatures, (f) is the average flow stress between the 2% and 6% strains for samples with different spacings at different temperatures.

The dislocation nucleation rate can be given by:

$$\vartheta = \vartheta_D exp\left(-\frac{Q_{(\sigma,T)}}{k_{B^T}}\right) \tag{3}$$

where ϑ_D is Debye frequency, k_B is the Boltzmann constant, T is temperature, and $Q_{(\sigma,T)}$ is the activation free energy which is determined by:

$$Q_{(\sigma,T)} = U - f_{(2)}\sigma V^* \tag{4}$$

where U is the activation enthalpy, σ is the stress on the system, V^* is the activation volume, and $f_{(2)}$ presents the stress concentration in the site between the GBs and TBs.

Substituting equations (2)–(4) into equation (1), we obtain:

$$\dot{\varepsilon} = f_{(1)}\beta\frac{d}{b}\frac{b}{\lambda}\vartheta_D exp(-\frac{U}{(k_BT)})\vartheta_D exp(-exp(-\frac{f_{(2)}\sigma V^*}{k_BT})). \tag{5}$$

For simplicity, $f_{(1)}\beta$ is taken as 1, then equation (5) is changed into:

$$\dot{\varepsilon} = \frac{b}{\lambda}\vartheta_D exp(-\frac{U}{(k_BT)})\vartheta_D exp(-exp(-\frac{f_{(2)}\sigma V^*}{k_BT})). \tag{6}$$

Then, the stress can be given as:

$$\sigma = \frac{U}{f_{(2)}V^*} - \frac{k_BT}{f_{(2)}V^*}\ln\left(\frac{d}{\lambda}\frac{\vartheta_D}{\dot{\varepsilon}}\right). \tag{7}$$

The first term on the right side describes the athermal stress, while the second term is the stress from the thermal contribution. Taking the value of parameters in table 1 into equation (7), the yield stress for samples with different λ at various temperatures can be calculated. The results are shown in figure 10, from which it can be seen that the yield stress for the sample with $\lambda \leqslant 1.83$ is well obtained from equation (7).

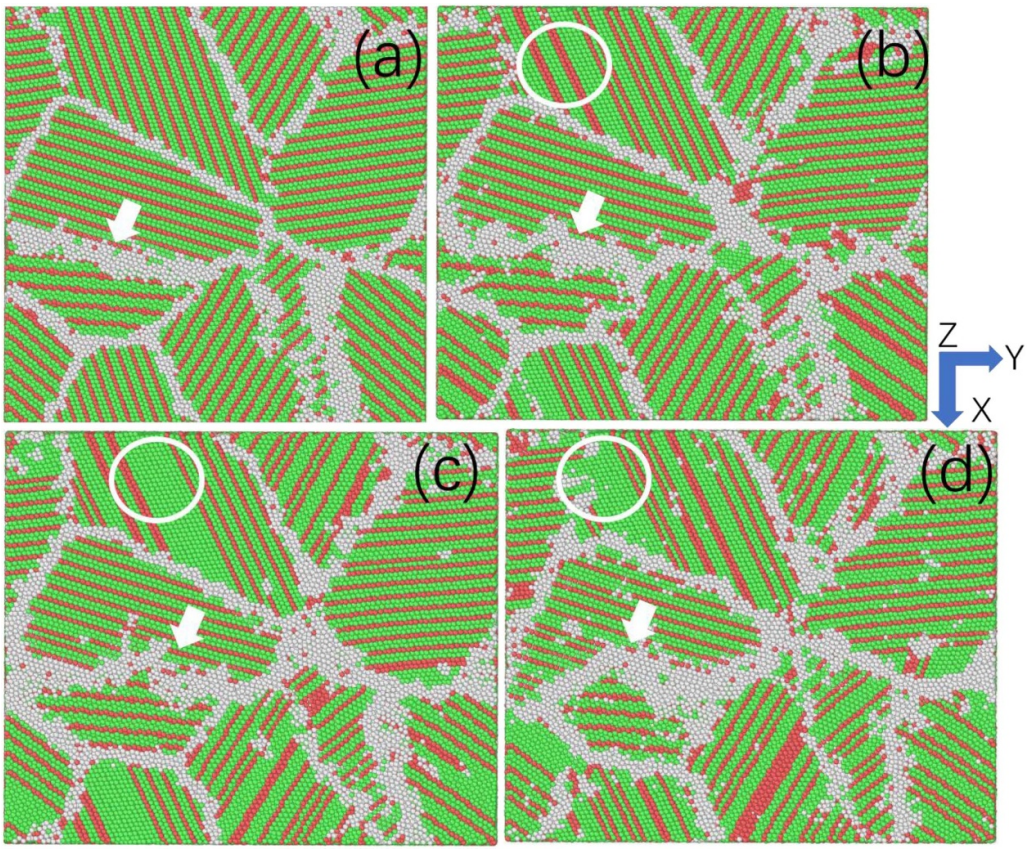

Figure 6. The deformation mechanism for the sample with $\lambda = 0.62$ nm at different temperatures. (a) The equilibrated state for the sample at 0.0 strain; (b)–(d) show the deformed states at temperatures of 1 K, 300 K, and 800 K, respectively. The areas in the white circles indicate the detwinning process, while white arrows indicate the migration of the GB.

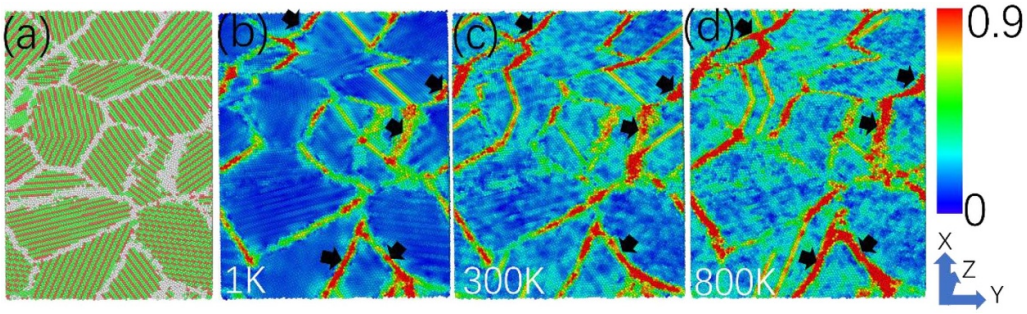

Figure 7. (a) The GBs are shown in white to illustrate their positions; (b)–(d) show the distribution of shear strain of the sample with $\lambda = 0.62$ nm at 1 K (b), 300 K (c), and 800 K (d). The shear strains near the GBs (indicated by dark arrows) increase clearly with increasing temperature.

For the sample with $\lambda \geqslant 1.83$ nm, the strengthening from λ can be quantitively expressed via the Hall–Petch relationship:

$$\sigma = \sigma_0 + \frac{k}{\sqrt{\lambda}} \tag{8}$$

where σ_0 is the intrinsic strengthening, k is the strengthening factor due to twin boundaries, and λ is the twin boundary spacing. By fitting the simulated results, the Hall–Petch curves for samples with different λ are illustrated in figure 10. Clearly, there are critical values of λ between the Hall–Petch curves and equation (7), as seen in the blue circles in figure 10. When λ is smaller than the critical value, the softening model (equation (7)) can be used to predict the yield stress, whereas the Hall–Petch relationship is more accurate for the sample with λ being greater than the critical value. Moreover, the critical values of λ obtained from theoretical modeling are very close to our simulation results, as demonstrated in figures 10(a)–(d).

5. Conclusions

In summary, the effect of TB spacing and temperature on the mechanical behavior of nanotwinned HEAs is systematically

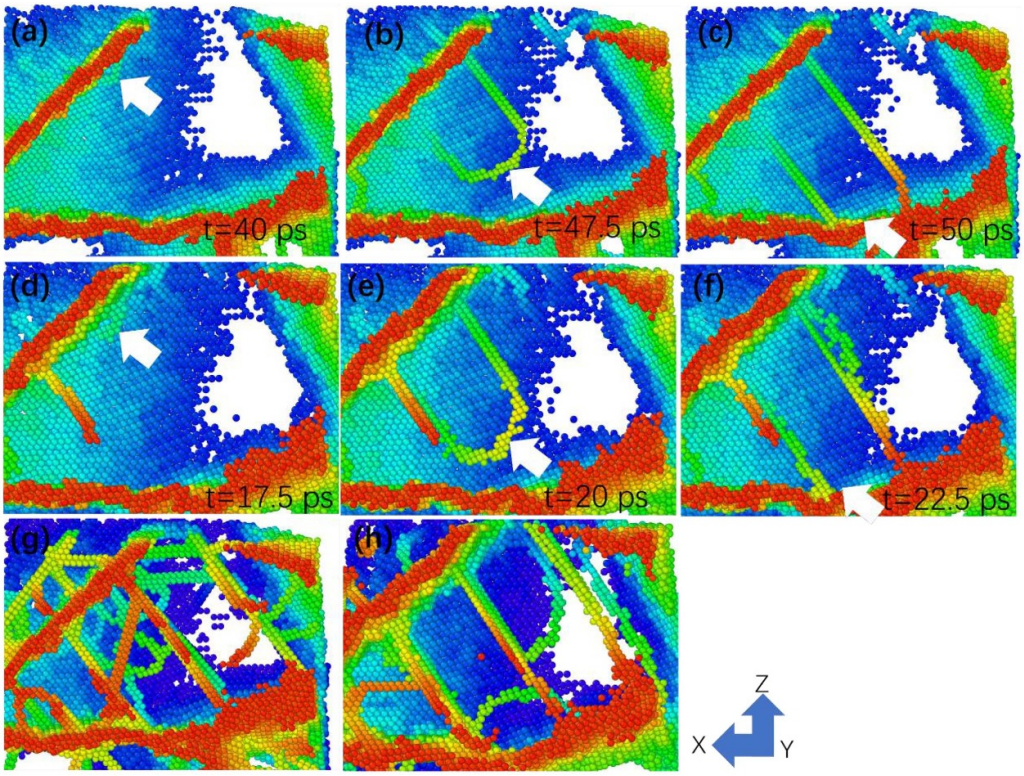

Figure 8. The dislocation behavior of one grain in the sample with $\lambda = 3.05$ nm at a temperature of 1 K (a)–(c), and a temperature of 300 K (d)–(f). The distribution of dislocations at 12% strain in one grain in the sample with $\lambda = 3.05$ nm at a temperature of 1 K (g) and 300 K (h). FCC and HCP atoms are not shown for clarity. The color of the atoms is given according to their spatial coordinate position.

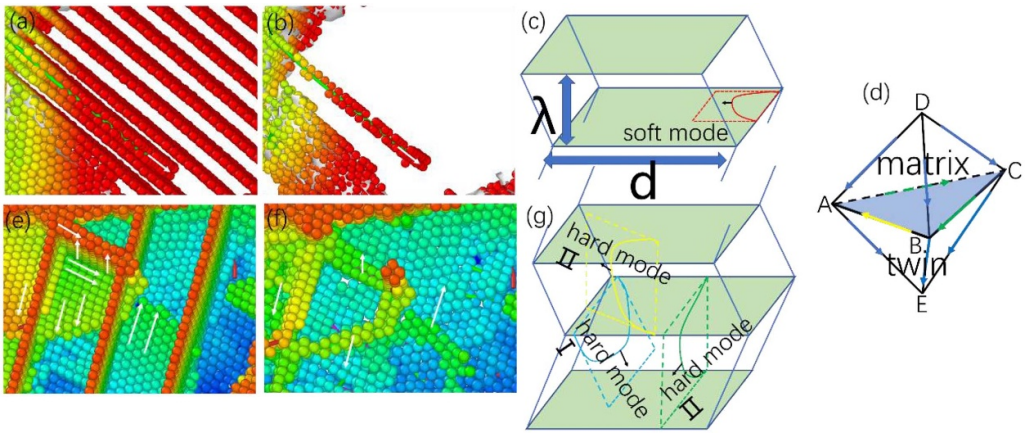

Figure 9. The deformation mechanisms in samples with different λ at 300 K, (a)–(c) show the soft-mode behavior of one dislocation in the sample with $\lambda = 0.61$ nm, (e)–(f) show two hardening-mode dislocation behaviors in the sample with $\lambda = 1.83$ nm, (d) is the double Thompson tetrahedra, which illustrates slip modes.

studied via MD simulation. The atomistic deformation mechanisms of nanotwinned HEAs are revealed in detail for samples with different twin boundary spacing (λ) at various temperatures. Based on the discussion above, some of the following conclusions can be drawn:

(1) λ-dependent strength of nanotwinned HEAs has been found in the MD simulation. When $\lambda \geqslant 1.83$ nm, the strength of nanotwinned HEAs is increased with decreased λ; when $\lambda < 1.83$ nm, the strength is decreased with reduced λ. This finding sheds light on the design of nanotwinned HEAs with high strength.

(2) In the sample with $\lambda < 1.83$ nm, dislocations nucleate from the junction between the grain boundary and twin boundary, then glide parallel to the TB. This soft-mode dislocation motion results in detwinning and a lack of dislocation interactions, and softening is found for the sample with $\lambda < 1.83$ nm.

(3) In the sample with $\lambda \geqslant 1.83$ nm, dislocations tend to interact with the TBs and travel in hardening-mode style, which

Table 1. Parameters used in the mechanistic model equation (7).

Parameter symbol	Description	Value	Origin
b	Magnitude of Burger vector	2.525 Å	[34]
λ	Twin boundary spacing	0.61 ~ 3.05 nm	Present study
d	Grain size	10 nm	Present study
ϑ_D	Debye frequency	10^{11} s^{-1}	[5]
$\dot{\varepsilon}$	Strain rate	10^{9} s^{-1}	Present study
U	Activation enthalpy	0.781 eV	Present study
V^*	Activation volume	74.83Å^3	Present study
$f(2)$	Stress concentration in the GB-TB junction	0.25 ~ 0.45	Present study
k_B	Boltzmann constant	1.380648×10^{-23} J/K	Present study
T	Temperature	1 K ~ 1200 K	Present study

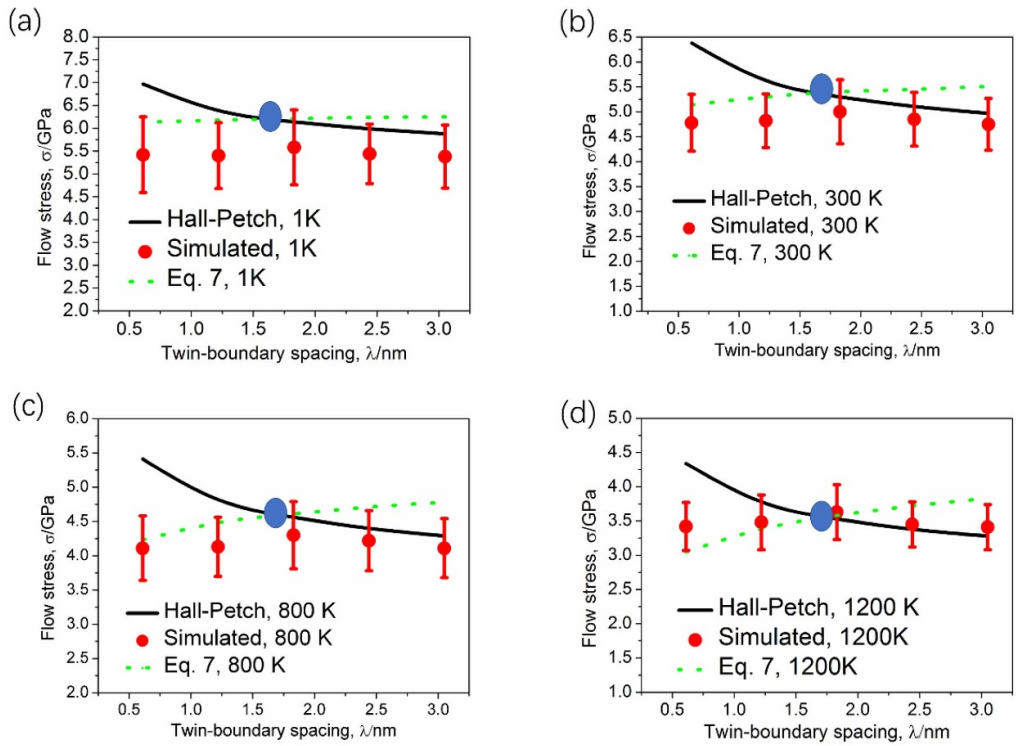

Figure 10. The yield stress of the nanotwinned CoCrFeNi alloy with different twin boundary spacings at different temperatures. The simulated results are well predicted by the mechanistic model shown in equation (7) and the Hall–Petch relationship. Further, the critical value of λ, illustrated by blue circles, is accurately obtained from the theoretical model.

leads to dislocation entanglements. Therefore, improved strength is found in samples with decreasing λ when $\lambda \geqslant 1.83$ nm.

(4) The dislocation motion at 1 K is slower than those at 300 K, leading to stronger dislocation entanglement at 1 K; GB migration is shown for samples deformed at higher temperature, shear strains are also much higher near GBs when the nanotwinned HEAs are deformed at high temperature.

(5) A mechanistic theoretical model combined with the Hall–Petch relationship, which takes the effect of λ and temperature into effect, is proposed to predict the yield stress and critical value of λ in nanotwinned HEAs.

Acknowledgments

The work was support by the National Natural Science Foundation, China (grant no. 11772204), the China Postdoctoral Science Foundation (grant no. 2019M661269), and the Guangdong Basic and Applied Basic Research Foundation (grant no. 2019A1515110887). Access to the National Computer Infrastructure in ANU is gratefully acknowledged.

ORCID iD

Zheng Zhong https://orcid.org/0000-0001-5293-7098

References

[1] Yan S, Zhou H, Xing B, Zhang S, Li L and Qin Q H 2018 Crystal plasticity in fusion zone of a hybrid laser welded Al alloys joint: from nanoscale to macroscale *Mater. Des.* **160** 313–24

[2] Yan S, Zhou H and Qin Q H 2019 Microstructure versus size nano microscale deformation of solute strengthening Al alloys via pillar compression tests *Mater. Res. Lett.* **7** 53–59

[3] Zhang Y, Zuo T T, Tang Z, Gao M C, Dahmen K A, Liaw P K and Lu Z P 2014 Microstructures and properties of high-entropy alloys *Prog. Mater. Sci.* **61** 1–93

[4] George E P, Raabe D and Ritchie R O 2019 High-entropy alloys *Nat. Rev. Mater.* **4** 515–34

[5] Ding Q *et al* 2019 Real-time nanoscale observation of deformation mechanisms in CrCoNi-based medium- to high-entropy alloys at cryogenic temperatures *Mater. Today* **25** 21–27

[6] Gludovatz B, Hohenwarter A, Catoor D, Chang E H, George E P, Ritchie R O 2014 A fracture-resistant high-entropy alloy for cryogenic applications *Science* **345** 1153–8

[7] Gwalani B, Soni V, Lee M, Mantri S A, Ren Y and Banerjee R 2017 Optimizing the coupled effects of Hall-Petch and precipitation strengthening in a Al 0.3 CoCrFeNi high entropy alloy *Mater. Des.* **121** 254–60

[8] Jin X, Liang Y, Zhang L, Bi J, Zhou Y and Li B 2019 Back stress strengthening dual-phase $AlCoCr_2FeNi_2$ high entropy alloy with outstanding tensile properties *Mater. Sci. Eng.* A **745** 137–43

[9] Li Z, Tasan C C, Springer H, Gault B and Raabe D 2017 Interstitial atoms enable joint twinning and transformation induced plasticity in strong and ductile high-entropy alloys *Sci. Rep.* **7** 40704

[10] Luo H, Li Z and Raabe D 2017 Hydrogen enhances strength and ductility of an equiatomic high-entropy alloy *Sci. Rep.* **7** 9892

[11] Lei Z *et al* 2018 Enhanced strength and ductility in a high-entropy alloy via ordered oxygen complexes *Nature* **563** 546–50

[12] Su J, Raabe D and Li Z 2019 Hierarchical microstructure design to tune the mechanical behavior of an interstitial TRIP-TWIP high-entropy alloy *Acta. Mater.* **163** 40–54

[13] Fu Z, MacDonald B E, Li Z, Jiang Z, Chen W, Zhou Y and Lavernia E J 2018 Engineering heterostructured grains to enhance strength in a single-phase high-entropy alloy with maintained ductility *Mater. Res. Lett.* **6** 634–40

[14] Nene S S, Liu K, Frank M, Mishra R S, Brennan R E, Cho K C, Li Z and Raabe D 2017 Enhanced strength and ductility in a friction stir processing engineered dual phase high entropy alloy *Sci. Rep.* **7** 16167

[15] Wu Z, Bei H, Pharr G and George E 2014 Temperature dependence of the mechanical properties of equiatomic solid solution alloys with face-centered cubic crystal structures *Acta. Mater.* **81** 428–41

[16] Ding Q *et al* 2019 Tuning element distribution, structure and properties by composition in high-entropy alloys *Nature* **574** 223–7

[17] Stepanov N, Tikhonovsky M, Yurchenko N, Zyabkin D, Klimova M, Zherebtsov S, Efimov A and Salishchev G 2015 Effect of cryo-deformation on structure and properties of CoCrFeNiMn high-entropy alloy *Intermetallics* **59** 8–17

[18] Lu K, Lu L and Suresh S 2009 Strengthening materials by engineering coherent internal boundaries at the nanoscale *Science* **324** 349–52

[19] Feng X B, Fu W, Zhang J Y, Zhao J T, Li J, Wu K, Liu G and Sun J 2017 Effects of nanotwins on the mechanical properties of Al x CoCrFeNi high entropy alloy thin films *Scr. Mater.* **139** 71–76

[20] Feng X, Fan S, Meng F, Surjadi J U, Cao K, Liao W and Lu Y 2019 Effect of Zr addition on microstructure and mechanical properties of CoCrFeNiZrx high-entropy alloy thin films *Appl. Nanosci.*

[21] Lu L, Chen X, Huang X and Lu K 2009 Revealing the maximum strength in nanotwinned copper *Science* **323** 607–10

[22] Pan Q, Zhou H, Lu Q, Gao H and Lu L 2017 History-independent cyclic response of nanotwinned metals *Nature* **551** 214–7

[23] Taheri Mousavi S M, Zhou H, Zou G and Gao H 2019 Transition from source- to stress-controlled plasticity in nanotwinned materials below a softening temperature *NPJ Comput. Mater.* **5** 2

[24] Hirel P 2015 Atomsk: A tool for manipulating and converting atomic data files *Comput. Phy. Commun.* **197** 212–9

[25] Plimpton S 1995 Fast parallel algorithms for short-range molecular dynamics *J. Comput. Phys.* **117** 1–19

[26] Qin Z, Qin Q H and Feng X-Q 2008 Mechanical property of carbon nanotubes with intramolecular junctions: molecular dynamics simulations *Phys. Lett.* A **372** 6661–6

[27] Cai K, Yin H, Qin Q H and Li Y 2014 Self-excited oscillation of rotating double-walled carbon nanotubes *Nano Lett.* **14** 2558–62

[28] Farkas D and Caro A 2018 Model interatomic potentials and lattice strain in a high-entropy alloy *J. Mater. Res.* **33** 3218–25

[29] Stukowski A 2010 Visualization and analysis of atomistic simulation data with OVITO–the open visualization tool *Modell. Simul. Mater. Sci. Eng.* **18** 1–7

[30] Yan S, Xing B and Qin Q H 2016 Effect of interface on the deformation of aluminium bicrystal: atomistic simulation study *MATEC Web Conf.* **82** 02010

[31] Li X, Wei Y, Lu L, Lu K and Gao H 2010 Dislocation nucleation governed softening and maximum strength in nano-twinned metals *Nature* **464** 877–80

[32] Zhu T, Li J, Samanta A, Leach A and Gall K 2008 Temperature and strain-rate dependence of surface dislocation nucleation *Phys. Rev. Lett.* **100** 025502-1–4

[33] Mason J K, Lund A C and Schuh C A 2006 Determining the activation energy and volume for the onset of plasticity during nanoindentation *Phys. Rev.* B **73** 1–14

[34] Varvenne C, Luque A and Curtin W A 2016 Theory of strengthening in fcc high entropy alloys *Acta. Mater.* **118** 164–76